Optics Letters

Tm³⁺ and Ho³⁺ colasing in in-band pumped waveguides fabricated by femtosecond laser writing

Esrom Kifle,[1,2] Pavel Loiko,[2] Carolina Romero,[3] ⓘ
Javier Rodríguez Vázquez de Aldana,[3] Viktor Zakharov,[4] Yulia Gurova,[4]
Andrey Veniaminov,[4] ⓘ Valentin Petrov,[5] Uwe Griebner,[5] Romain Thouroude,[2]
Mathieu Laroche,[2] Patrice Camy,[2] Magdalena Aguiló,[1] Francesc Díaz,[1] and
Xavier Mateos[1,*] ⓘ

[1] *Universitat Rovira i Virgili (URV), Física i Cristal·lografia de Materials i Nanomaterials (FiCMA-FiCNA), Marcel.li Domingo 1, 43007 Tarragona, Spain*
[2] *Centre de Recherche sur les Ions, les Matériaux et la Photonique (CIMAP), UMR 6252 CEA-CNRS-ENSICAEN, Université de Caen Normandie, 6 Boulevard du Maréchal Juin, 14050 Caen Cedex 4, France*
[3] *Aplicaciones del Láser y Fotónica, University of Salamanca, 37008 Salamanca, Spain*
[4] *ITMO University, 49 Kronverkskiy Pr., 197101 St. Petersburg, Russia*
[5] *Max-Born-Institute for Nonlinear Optics and Short-Pulse Spectroscopy, 2A Max-Born-Str., D-12489 Berlin, Germany*
*Corresponding author: xavier.mateos@urv.cat

We report on the first, to the best of our knowledge, in-band pumped Tm³⁺, Ho³⁺ codoped waveguide (WG) laser. A depressed-index surface channel WG (type III) with a 50 μm half-ring cladding is fabricated in a 5 at. % Tm³⁺, 0.5 at. % Ho³⁺ : KLu(WO₄)₂ crystal by femtosecond pulse direct laser writing. Under in-band pumping by a 1679 nm Er Raman fiber laser, Tm³⁺ and Ho³⁺ colasing is observed in the WG and explained by bidirectional energy transfer. The maximum total output power at ∼1942 nm (Tm³⁺) and 2059 nm (Ho³⁺) is 448 mW with a slope efficiencyM of 40.6%, which is a record high for this type of WG lasers. The maximum output power of the Ho laser reaches 144 mW.   © 2020 Optical Society of America

The Holmium ion (Ho³⁺) is attractive for solid-state laser emission at wavelengths slightly above 2 μm ($^5I_7 \rightarrow {}^5I_8$ transition), falling in the eye-safe spectral range. Ho lasers are of practical interest for remote sensing, wind mapping, medicine, and further frequency conversion into the mid-IR. A common way to excite the Ho³⁺ ions is codoping of the host matrix with thulium (Tm³⁺) ions acting as sensitizers [1,2]. Tm³⁺ ions can be pumped at ∼0.8 μm (to the $^3H_4$ state), transferring a part of the energy of the electronic excitation to the Ho³⁺ ones via nonradiative energy transfer (ET), and Tm³⁺($^3F_4$) → Ho³⁺($^5I_7$) [3] and such codoped *bulk* lasers can be very efficient [1]. A diode-pumped Tm, Ho : KLu(WO₄)₂ (Tm,Ho:KLuW) laser generated an output power of 451 mW at 2081 nm with a slope

efficiency of 31% [2]. Tm³⁺, Ho³⁺ codoped materials are also attractive for mode-locked lasers at >2 μm [4,5]. Their emission wavelength is red-shifted (with respect to single Tm³⁺ doping), avoiding the structured water vapor absorption, and the combined gain bandwidth is broader favoring sub-100-fs pulses [4,5].

Optically "passive" surface WGs supporting light guiding at ∼2 μm could find applications in bio- and environmental sensing based on evanescent-field interaction with materials on the surface. The probing of "passive" WGs can be provided by another integrated ("active") device. "Active" surface WGs are also suitable for pulsed sources based on interaction with a surface-deposited saturable absorber [6]. Efficient surface Tm³⁺, Ho³⁺ WG lasers with a broadband emission around 2 μm are excellent candidates for these aims. Unfortunately, so far, only a few studies have been devoted to this topic [7–9]. Planar Tm³⁺, Ho³⁺ codoped WGs based on KY(WO₄)₂ and LiYF₄ layers grown by liquid phase epitaxy (LPE) are known [7,8]. A Tm, Ho : LiYF₄ planar WG laser is generated 81 mW at 2051 nm with a slope efficiency of 24% [8]. In [9], buried channel WGs were fabricated in bulk Tm, Ho:ZBLAN glass by femtosecond direct laser writing (fs-DLW), yielding 76 mW at 2052 nm with a similar slope. Note that in all of these publications, the conventional pump scheme (excitation to the $^3H_4$ level of Tm³⁺) was used.

The difficulty in developing Tm³⁺, Ho³⁺ lasers is the strong thermal effect [2] due to energy losses occurring in the following processes: relaxation of Tm³⁺ ions to the $^3F_4$ state, possible Ho³⁺ → Tm³⁺ back ET, and ET upconversion (ETU). In part, it can be alleviated by (in-band) pumping of Tm³⁺ to the $^3F_4$
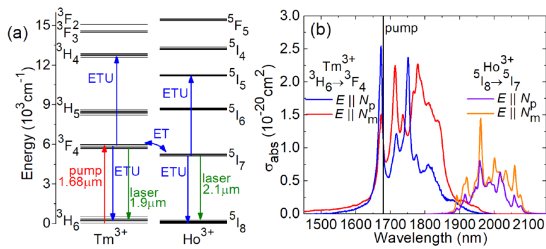
Fig. 1. In-band pumping of Tm, Ho:KLuW: (a) energy-level scheme of Tm^{3+} and Ho^{3+}: *red (green) arrow*, pump (laser) transition; ET, energy-transfer; ETU, ET upconversion; (b) absorption cross sections, σ_{abs}, for the $^3H_6 \rightarrow {}^3F_4 Tm^{3+}$ and $^5I_8 \rightarrow {}^5I_7 Ho^{3+}$ transitions and light polarized along the N_p and N_m optical indicatrix axes.

state, Fig. 1(a). *Bulk* in-band pumped Tm^{3+}, Ho^{3+} lasers are known [10]. Recently, we reported the first singly Tm-doped in-band pumped channel WG laser delivering up to 2.05 W at 1881 nm with a record-high slope efficiency of 78.3% [11]. In the present work, we demonstrate the first in-band pumped Tm^{3+}, Ho^{3+} codoped WG laser.

As a gain material, we employed monoclinic 5 at. % Tm, 0.5 at. % Ho:KLuW grown by the top seeded solution growth method using $K_2W_2O_7$ as a solvent. The actual Tm^{3+} and Ho^{3+} doping levels were determined by electron probe microanalysis to be $N_{Tm} = 2.30 \times 10^{20}$ cm^{-3} and $N_{Ho} = 0.53 \times 10^{20}$ cm^{-3}. A rectangular sample was cut in the frame of the optical indicatrix of KLuW. The uncoated sample was 3.0-mm-thick along the N_g axis. Its $5.8(N_m) \times 1.5(N_p)$ mm^2 input and output faces and the top surface were polished.

Depressed-index guides with a half-ring cladding (type III) were fabricated by fs-DLW. To produce individual damage tracks, the output of a Ti:sapphire regenerative amplifier (Spitfire, Spectra Physics) delivering 120 fs (795 nm central wavelength) at 1 kHz repetition rate was focused into the bulk volume of the material through the top surface ($N_m \times N_g$). Only a small fraction of the pulse energy was employed (65 nJ). The writing optics comprised a $40\times$ microscope objective (numerical aperture, N.A. = 0.65). The crystal was scanned at a speed of 500 µm/s along its N_g axis, resulting in the formation of the damage tracks. The polarization of the fs laser was perpendicular to the writing direction ($\boldsymbol{E} \| N_m$). No repolishing after the inscription of the damage tracks was applied.

The geometry of the guides was inspected using a confocal laser microscope (LSM 710, Carl Zeiss). The resolution was 0.24 µm. The end-facet view with polarized light ($P \| N_p$) in bright field, Fig. 2(a), reveals a half-ring cladding formed by 31 vertically elongated damage tracks. The diameter of the cladding is ~50 µm, and the upper/lower tracks are located at 12/49 µm beneath the crystal surface. The cross-section size of each track is $1 (N_m) \times 6 (N_p)$ µm^2, and their separation is 2 µm (horizontal). No macroscopic cracks in the core or in the surrounding bulk area are observed. The inspection of the same area in the dark field, Fig. 2(b), reveals bright scattering centers coinciding with the written tracks. The top view with polarized light ($P \| N_g$), Fig. 2(c), indicates that the damage tracks are continuous, and they propagate through the entire length of the sample reaching the end facets at both sides. The cladding resembles a canvas-like structure. Individual tracks are visualized in Fig. 2(d), showing dark borders and a brighter inner part
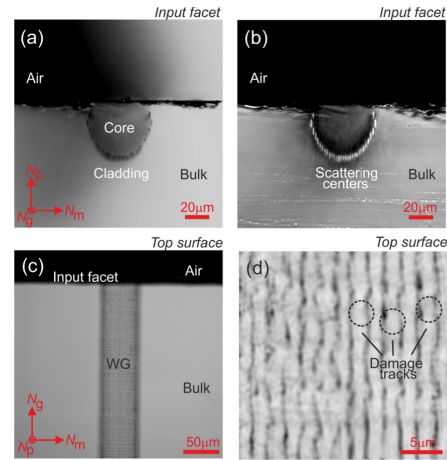

Fig. 2. Confocal microscopy study of the fs-DLW Tm^{3+}, Ho^{3+} codoped channel WGs: (a), (b) end-facet view—(a) bright and (b) dark field; (c), (d) top surface view in bright field—(c) area adjacent to the input facet, (d) individual damage tracks. Transmission mode, polarized light P: (a), (b) P$\| N_p$; (c), (d) P$\| N_g$. λ = 405 nm.

probably due to local expansion and partial amorphization of the material subjected to the fs temporal structure of the pulses.

To study the effect of the fs laser writing irradiation on the emission properties of rare-earth ions (Tm^{3+} and Ho^{3+}), the intensity of the green Ho^{3+} emission was monitored across the end-facet area, Fig. 3(a). It revealed a clear drop in the emission intensity within the cladding and almost unchanged luminescence response of the core. A close look at the individual damage tracks from the top surface, Fig. 3(b), indicated a strong localization of the depressed emission intensity within the dark "sidewalls" of the tracks.

Using a confocal Raman microscope, (InVia, Renishaw) equipped with a $50\times$ objective, we measured the micro-luminescence spectra from the core region for
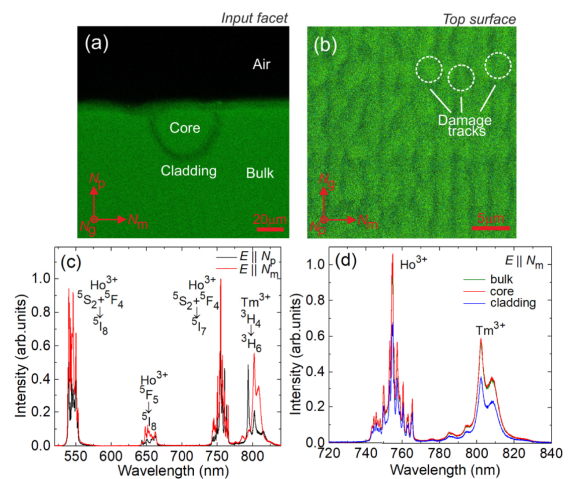

Fig. 3. µ-luminescence study of the fs-DLW Tm^{3+}, Ho^{3+} codoped channel WGs: (a), (b) µ-luminescence mapping—(a) end-facet view, (b) top view with a closer look at the damage tracks. $^5S_2 + {}^5F_4 \rightarrow {}^5I_8 Ho^{3+}$ emission, unpolarized light; (c) polarized emission spectra from the core region for $\boldsymbol{E} \| N_p$ and $\boldsymbol{E} \| N_m$; (d) comparison of the emission spectra from the bulk, core, and cladding regions, $\boldsymbol{E} \| N_p$. λ_{exc} is 488 nm.

$E \parallel N_p$ and $E \parallel N_m$, Fig. 3(c). This confirmed well-preserved anisotropy of the spectroscopic properties of the material in the core region. By focusing the radiation on three areas (focus diameter: 2 μm) in the bulk material, in the WG core, and on the WG cladding, we compared the emission spectra of $Ho^{3+}(^5S_2 + ^5F_4 \rightarrow ^5I_7)$ and $Tm^{3+}(^3H_4 \rightarrow ^3H_6)$ ions. As shown in Fig. 3(d), there is no reduction in intensity or alteration of the spectral shape for the core region. The emission intensity is depressed in the cladding, while only slight changes in the spectral shape (e.g., peak shifts and broadening) are detected. It suggests a strongly spatially localized alteration of the crystal field around the rare-earth ions.

The laser experiments were performed in a linear plano-plano laser cavity containing a pump mirror (PM) coated for high transmission (HT) at the pump wavelength ($T = 93\%$ at 1.68 μm), high reflection (HR) at 1.87–2.30 μm, and a set of output couplers (OCs) with an actual transmission at the laser wavelength T_{OC} in the range of 1.5%n20%. OCs with higher transmissions ($T_{OC} = 30\% - 50\%$) resulted only in Tm^{3+} lasing with deteriorated performance, and, thus, they were not studied. Both cavity mirrors were gently pressed towards the crystal end facets (without any index-matching liquid), leading to a geometrical cavity length of 3.0 mm. The sample was fixed on a Cu holder using a silver paint.

The pump source was a Raman fiber laser (RFL) [11]. It was comprised of a 1560 nm erbium master-oscillator power amplifier and a polarization-maintaining GeO_2-doped silica fiber with a Raman-active mode at 440 cm^{-1}. The RFL delivered 4.0 W at 1679 nm (emission bandwidth: 1 nm) linearly polarized and a spatially single-mode output ($M^2 < 1.1$). The pump wavelength corresponded to the $^3H_6 \rightarrow ^3F_4 Tm^{3+}$ transition, Fig. 1(b). The pump was focused through the PM using a spherical uncoated CaF_2 lens ($f = 40$ mm, $T = 94\%$). The measured pump spot at the input WG facet $2w_P$ was 30 ± 5 μm. The pump polarization corresponded to $E \parallel N_m$. More details can be found elsewhere [11].

The pump coupling efficiency $\eta_{coupl} = P_{coupl}/P_{inc} \approx 89\%$ was simply estimated from Fresnel losses (refractive index $n_m = 2.002$) because the pump spot size is smaller than the WG dimensions, and the condition $(N.A.)_{pump} < (N.A)_{WG} \approx 0.05$ was satisfied. The absorption under non-lasing conditions, $\eta_{abs,NL} = P_{abs}/P_{coupl}$, was determined from measurements of the transmitted pump. A strong absorption bleaching was detected: $\eta_{abs,NL}$ gradually decreased below its small-signal value, $\eta_{abs,0} = 1 - \exp(-\sigma_{abs}^P N_{Tm} t) = 50.9\%$, where $\sigma_{abs}^P = 1.03 \times 10^{-20}$ cm^2 and $t = 3.0$ mm, Fig. 1(b). The small-signal single-pass pump absorption length was 4.2 mm. The absorption under lasing conditions, $\eta_{abs,L}$, was calculated from the $\eta_{abs,NL}$ value at the threshold pump power for each OC, accounting for the double pass of the pump because the OCs were highly reflective at ~1.68 μm. The $\eta_{abs,L}$ value obtained in the range $42 - 49 \pm 1\%$ (depending on the OC) ensured almost uniform pumping (inversion) in the WG [8].

The output beam was collimated with an uncoated CaF_2 lens ($f = 15$ mm), and a cutoff filter ($T < 0.001\%$ at ~1.68 μm) was used to filter out the residual pump. An optical spectrum analyzer (OSA, AQ6375B, Yokogawa) equipped with a multimode low-OH optical fiber that served for recording the emission spectra. The laser beam profile was captured using a FIND-R-SCOPE near-IR camera; the scale was calibrated by illuminating WGs with a known size.

The output dependences of the Tm, Ho WG laser are shown in Fig. 4(a). For all the studied OCs, colasing of $Tm^{3+}(^3F_4 \rightarrow ^3H_6$ transition) and $Ho^{3+}(^5I_7 \rightarrow ^5I_8$ transition) ions was observed. Thus, we first measured the total ($\Sigma = Tm + Ho$) power. The maximum power was 448 mW at ~1942 nm (Tm^{3+}) and 2059 nm (Ho^{3+}) with a slope efficiency η_Σ of 40.6% (versus P_{abs}) ($T_{OC} = 9\%$). The laser threshold occurred at $P_{abs} = 334$ mW, and the optical-to-optical efficiency $\eta_{opt,\Sigma}$ was 28.2% (versus P_{inc}). The laser threshold increased with T_{OC}, from $P_{abs} = 120$ mW ($T_{OC} = 1.5\%$) to 366 mW ($T_{OC} = 20\%$).

The laser emission for the studied OCs was linearly polarized ($E \parallel N_m$, horizontal), and the polarization state was naturally selected by the gain anisotropy for both Tm^{3+} and Ho^{3+} transitions. Typical spectra are shown in Fig. 4(b). The Ho^{3+} laser wavelength (~2059 nm) was almost independent on T_{OC}; the Tm^{3+} emission occurred between 1915–1963 nm, showing a tendency for a blue shift with increasing the T_{OC} due to the quasi-three-level Tm laser scheme with reabsorption.

The wavelength difference for Tm^{3+} and Ho^{3+} allowed for separating the corresponding power fractions using a dichroic mirror, e.g., that for the Ho^{3+} part: Ho/(Ho + Tm), Fig. 4(c). Both the Ho^{3+} power fraction, and the output power, $P_{out,Ho}$, showed a complex dependence on the output coupling. The maxima for these parameters occurred at the same intermediate $T_{OC} = 5\%$ [Ho/(Ho + Tm) = $84 \pm 4\%$]. For higher T_{OC}, both parameters gradually decrease to zero [for $T_{OC} = 20\%$, Ho/(Ho + Tm) < 1%]. Thus, the maximum Ho^{3+} output power is observed for $T_{OC} = 5\%$, amounting to 144 mW. Note that for this OC the total (Tm + Ho) characteristics are 174 mW at 1916 nm (Tm^{3+}) and 2059 nm (Ho^{3+}) with $\eta_\Sigma = 15.1\%$ and a laser threshold of 206 mW. The minimized Tm power fraction for this OC corresponding to a wavelength of 1916 nm can explain this blue shift of the Tm^{3+} emission.
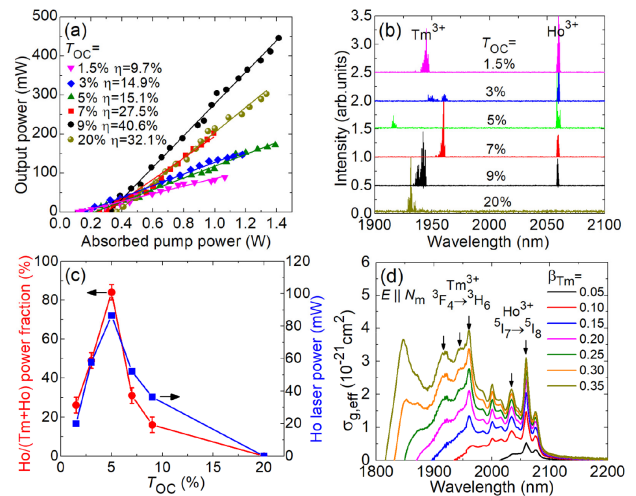

Fig. 4. CW in-band pumped Tm^{3+}, Ho^{3+} codoped surface channel WG laser: (a) input–output dependences, η, slope efficiency; (b) emission spectra, $P_{abs} = 0.9$ W; (c) relative power fraction of Ho^{3+} emission, Ho/(Tm + Ho), and the Ho^{3+} output power versus output coupling, $P_{abs} = 0.9$ W; (d) effective gain cross sections, $\sigma_{g,eff}$, for different Tm^{3+} inversion ratios $\beta_{Tm} = N_2(^3F_4)/N_{Tm}$, *arrows* indicate the observed laser wavelengths. The laser polarization is $E \parallel N_m$.
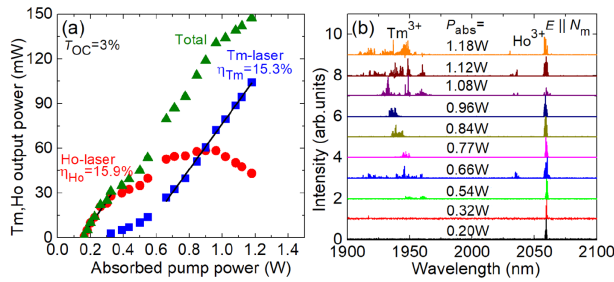
Fig. 5. Power and spectral properties of Tm^{3+} and Ho^{3+} emissions from the in-band pumped Tm^{3+}, Ho^{3+} codoped channel WG laser: (a) input–output dependences, $\eta_{Tm(Ho)}$, slope efficiency for Tm^{3+}- and Ho^{3+}-lasing, respectively; (b) laser emission spectra. The laser polarization is $\boldsymbol{E} \parallel N_m$.
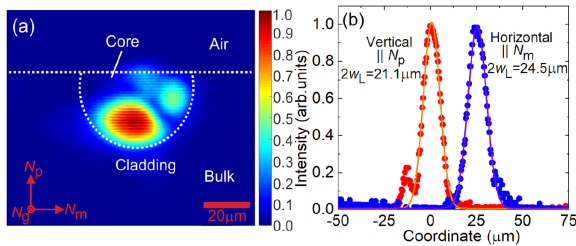

Fig. 6. Near-field intensity profile of the Ho lasing mode: (a) two-dimensional (2D) mode profile, where dashed lines indicate the crystal/air interface and the WG cladding; (b) one-dimensional (1D) intensity plots along the horizontal ($\parallel N_m$) and vertical ($\parallel N_p$) directions, symbols, experimental data; *curves*, Gaussian fits. The laser polarization, $\boldsymbol{E} \parallel N_m$, is horizontal. $T_{OC} = 5\%$, $P_{abs} = 1.0$ W.

The example power dependence of the Tm^{3+} and Ho^{3+} WG laser is illustrated in Fig. 5 for $T_{OC} = 3\%$. Note the slightly nonlinear dependence explained by power redistribution between Tm^{3+} and Ho^{3+} lasing. The threshold is much lower for the Ho^{3+} laser (161 mW) than for Tm^{3+} (320 mW). The Ho^{3+} power first increases linearly with a slope efficiency η_{Ho} of 15.9%. As soon as the threshold for Tm^{3+} lasing is reached, its power increases nonlinearly at the expense of the Ho^{3+} one. The corresponding slope efficiency η_{Tm} is 15.3%, obtained by fitting the output dependence well above the Tm^{3+} laser threshold. The laser spectra, Fig. 5(b), broaden with very pronounced increases in the pump power for the Tm emission.

The Tm^{3+} and Ho^{3+} emission channels both produced a spatially multimode output. The typical near-field profile of the Ho laser is shown in Fig. 6(a). More than 75% of the power was contained in the main lobe. It had an asymmetric shape and it was localized non-symmetrically with respect to the cladding adjacent to its bottom. The lobe had nearly Gaussian intensity profiles in the horizontal and vertical directions, Fig. 6(b), corresponding to the mode diameters $2w_L$ of 24.5 µm ($\parallel N_m$) and 21.1 µm ($\parallel N_p$).

To explain the observed colasing, we calculated the effective gain cross sections, $\sigma_{g,eff}$, for the Tm^{3+}, Ho^{3+}-codoped KLuW crystal:

$$\sigma_{g,eff} = \sigma_{g,Ho}\,(N_{Ho}/N_{\Sigma}) + \sigma_{g,Tm}\,(N_{Tm}/N_{\Sigma}), \qquad \textbf{(1a)}$$

$$\sigma_{g,Tm(Ho)} = \beta_{Tm(Ho)}\sigma_{SE,Tm(Ho)} - (1 - \beta_{Tm(Ho)})\sigma_{abs,Tm(Ho)}. \qquad \textbf{(1b)}$$

Here, $\beta_{Tm} = N_2(^3F_4)/N_{Tm}$ and $\beta_{Ho} = N_7(^5I_7)/N_{Ho}$ are the inversion levels for Tm^{3+} and Ho^{3+} ions, respectively, σ_{SE} and σ_{abs} are the stimulated emission and absorption cross sections, respectively, for both the $^3F_4 \leftrightarrow {}^3H_6$ Tm^{3+} and $^5I_7 \leftrightarrow {}^5I_8$ Ho^{3+} transitions, and $N_{\Sigma} = N_{Tm} + N_{Ho}$. The relation between β_{Tm} and β_{Ho} was determined, accounting for the parameters of the bidirectional $Tm^{3+} \leftrightarrow Ho^{3+}$ ET [3]. For low $\beta_{Tm} < 0.20$, the local peaks at 2075 and 2059 nm are assigned to Ho^{3+} emission. For higher inversion levels (β_{Tm} and, accordingly, β_{Ho}), the peaks at 1915, 1946, and 1960 nm (Tm^{3+}) and at 2034 and 2059 nm (Ho^{3+}) dominate and correspond to close gain, leading to Tm^{3+}, Ho^{3+} colasing.

To conclude, the combination of fs-DLW to fabricate surface channel WGs in anisotropic crystals and in-band pumping by a RFL to alleviate thermal issues is a novel approach for the development of integrated light sources emitting at ~2 µm. We report on a record-high Ho^{3+} output from a Tm^{3+}, Ho^{3+} codoped WG laser. Single Ho^{3+} emission will be possible at lower propagation losses (lower β) and lower Ho/Tm ratios.

Disclosures. The authors declare no conflicts of interest.

REFERENCES

1. G. L. Bourdet and G. Lescroart, Appl. Opt. **38**, 3275 (1999).
2. P. Loiko, J. M. Serres, X. Mateos, K. Yumashev, N. Kuleshov, V. Petrov, U. Griebner, M. Aguiló, and F. Díaz, Opt. Express **22**, 27976 (2014).
3. B. M. Walsh, N. P. Barnes, and B. Di Bartolo, J. Lumin. **90**, 39 (2000).
4. Y. Zhao, Y. Wang, X. Zhang, X. Mateos, Z. Pan, P. Loiko, W. Zhou, X. Xu, J. Xu, D. Shen, S. Suomalainen, A. Härkönen, M. Guina, U. Griebner, and V. Petrov, Opt. Lett. **43**, 915 (2018).
5. Y. Zhao, Y. Wang, W. Chen, Z. Pan, L. Wang, X. Dai, H. Yuan, Y. Zhang, H. Cai, J. E. Bae, S. Y. Choi, F. Rotermund, P. Loiko, J. M. Serres, X. Mateos, W. Zhou, D. Shen, U. Griebner, and V. Petrov, Opt. Express **27**, 1922 (2019).
6. E. Kifle, P. Loiko, J. R. V. de Aldana, A. Ródenas, S. Y. Choi, F. Rotermund, V. Zakharov, A. Veniaminov, M. Aguiló, F. Díaz, U. Griebner, V. Petrov, and X. Mateos, Photon. Res. **6**, 971 (2018).
7. C. V. Ruiz Madroñero, X. Mateos, P. Loiko, V. Petrov, U. Griebner, M. Aguiló, and F. Díaz, Laser Phys. Lett. **13**, 095801 (2016).
8. P. Loiko, R. Soulard, G. Brasse, J.-L. Doulan, A. Braud, A. Tyazhev, A. Hideur, and P. Camy, Opt. Lett. **43**, 4341 (2018).
9. D. G. Lancaster, S. Gross, H. Ebendorff-Heidepriem, A. Fuerbach, M. J. Withford, and T. M. Monro, Opt. Lett. **37**, 996 (2012).
10. Y. L. Kalachev, V. A. Mikhailov, V. V. Podreshetnikov, and I. A. Shcherbakov, Quantum Electron. **40**, 296 (2010).
11. P. Loiko, R. Thouroude, R. Soulard, L. Guillemot, G. Brasse, J.-L. Doualan, B. Guichardaz, A. Braud, A. Hideur, M. Laroche, H. Gilles, and P. Camy, Opt. Lett. **44**, 3010 (2019).